BULLETIN OF THE POLISH ACADEMY OF SCIENCES
TECHNICAL SCIENCES
Vol. 54, No. 3, 2006

Assessment of direct torque control for induction motor drives

D. CASADEI*, G. SERRA, A. TANI, and L. ZARRI

Dipartimento di Ingegneria Electtrica, Universita' di Bologna, 2 Viale Risogimento, 40136 Bologna, Italia

Abstract. Among all control methods for induction motor drives, Direct Torque Control (DTC) seems to be particularly interesting being independent of machine rotor parameters and requiring no speed or position sensors. The DTC scheme is characterized by the absence of PI regulators, coordinate transformations, current regulators and PWM signals generators. In spite of its simplicity, DTC allows a good torque control in steady state and transient operating conditions to be obtained. However, the presence of hysteresis controllers for flux and torque could determine torque and current ripple and variable switching frequency operation for the voltage source inverter. This paper is aimed to analyze DTC principles, the strategies and the problems related to its implementation and the possible improvements.

Key words: direct torque control, induction motor drive, stator flux vector control, flux weakening.

1. Introduction

In recent years, the commercial applications of the Field-Oriented Control (FOC) of Induction Motor (IM) drives have greatly increased. A number of studies has been developed to find out different solutions for the control of the IM drives with two objectives, namely i) fulfilment of the requirements for a precise and quick control of the motor flux and torque, and ii) reduction of the complexity of the algorithms involved in a FOC.

A new technique for the torque control of induction motors was developed and presented by I. Takahashi as Direct Torque Control (DTC) [1–3], and by M. Depenbrock as Direct Self Control (DSC) [4–6]. Since the beginning, the new technique was characterized by simplicity, good performance and robustness [1–17]. The basic scheme of DSC is preferable in the high power range applications, where a lower inverter switching frequency can justify higher current distortion.

Differently from FOC, DTC does not tend to reproduce the electromechanical behaviour of a dc motor drive but is aimed at a complete exploitation of the flux and torque-producing capabilities of an IM fed by a Voltage Source Inverter (VSI).

The DTC scheme is characterized by the absence of PI regulators, coordinate transformations, current regulators and PWM signals generators.

This paper concerns DTC, the strategies and the problems related to its implementation.

Some basic relationships regarding the space vector representation of three-phase quantities, the induction motor equations and VSI description are shown in Appendix.

The basic principles of flux and torque control and the switching table are firstly presented in order to accomplish the DTC concept. The switching strategies as well as the influence of the torque and flux hysteresis band amplitude on the drive behaviour are then shown. A particular attention has been made on the analytical relationship between the applied voltage and the corresponding torque variation in a cycle period.

Then, the DSC strategy and some improvement to the basic DTC scheme are analyzed.

Finally, a new technique for flux weakening implementation in DTC drive is analyzed and a comparison between DTC and FOC is presented.

2. Flux control principles

Let us consider an IM supplied by a VSI. If an inverter configuration is maintained during a time interval Tc, it is possible to determine the effect of the inverter configuration on the stator flux. From the stator voltage equation written in a stator reference frame we obtain

$$\frac{d\bar{\varphi}_s}{dt} = \bar{v}_s - R_s\,\bar{i}_s \tag{1}$$

where

$$|\bar{v}_s| = \begin{cases} {}^2\!/_3\,V_C & \text{active configs.} \\ 0 & \text{null configs.} \end{cases} \tag{2}$$

Assuming the voltage drop on the stator resistance small, (1) can be rewritten as

$$\frac{d\bar{\varphi}_s}{dt} \cong \bar{v}_s. \tag{3}$$

Then, for small values of T_c the stator flux at $(k+1)$th sampling instant can be calculated as

$$\bar{\varphi}_{s_{k+1}} = \bar{\varphi}_{s_k} + \bar{V}_k\,T_C \tag{4}$$

being k the index of the configuration applied at k-th instant.

It can be noted that the selection of a null configuration in a cycle period stops the stator flux space vector in the d-q plane. Instead, the selection of an active configuration in a cycle period moves the stator flux space vector along the direction of the applied stator voltage. The distance covered from the stator flux space vector in a cycle period is proportional to V_C and T_c, being

$$\left|\bar{\varphi}_{s_{k+1}} - \bar{\varphi}_{s_k}\right| = \frac{2}{3} V_C\,T_C. \tag{5}$$

*e-mail: domenico.casadei@mail.ing.unibo.it

With an opportune selection of the sequence of the inverter configurations the stator flux space vector can be driven along any trajectory, with a prefixed average speed.

A smaller value of the cycle period allows a more regular trajectory to be obtained, as shown in Fig. 1.

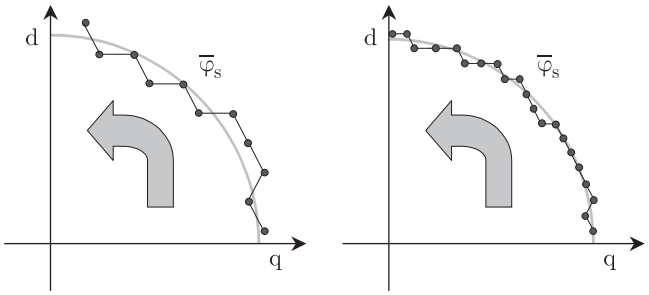

Fig. 1. Stator flux trajectories with different values of the cycle period T_c

If a hysteresis comparator is used to control the flux, the flux hysteresis band becomes the circular region in the d-q plane emphasized in Fig. 2. In order to drive the flux within the hysteresis band, the VSI applies to the motor the suitable voltage vector in a cycle period. The radial component of the voltage acts on the flux magnitude, while the tangential component determines the vector rotation (see Fig. 2).

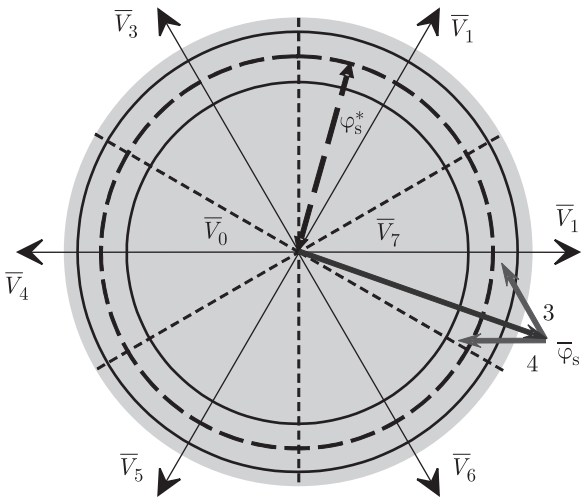

Fig. 2. Flux hysteresis band in the d-q plane and schematic representation of the flux vector variations due to the application of two different voltage vectors

The criterion of selection of the inverter configuration for the flux magnitude control is intuitive. It is based on the knowledge of the stator flux sector (Fig. 2). In general, at least 2 inverter configurations satisfy the criterion. As it will be shown in the next Section, this degree of freedom can be utilized in order to control the produced torque.

3. Torque control principle

If an inverter configuration is maintained during a time interval T_c, it is possible to determine the effect of the inverter configuration on the motor torque.

From the IM equations, written in a rotor reference frame, we can obtain

$$\frac{d\bar{\varphi}_r}{dt} = -\frac{1}{\sigma\,\tau_r}\,\bar{\varphi}_r + \frac{M}{\sigma\,\tau_r\,L_s}\,\bar{\varphi}_s^r \tag{6}$$

where

$$\sigma = 1 - \frac{M^2}{L_s L_r}, \qquad \tau_r = \frac{L_r}{R_r}.$$

The relationship (6) is a linear differential equation of the first order describing the behaviour of the rotor flux as a function of the stator flux.

Rewriting (6) using the Laplace transform gives

$$\bar{\varphi}_r = \frac{M/L_s}{1+\sigma\,\tau_r\,s}\,\bar{\varphi}_s^r. \tag{7}$$

Equation (7) shows that the relation between the stator flux and the rotor flux represents a low pass with time constant $\sigma\tau_r$. A sudden variation of the stator flux is followed with a delay from the rotor flux.

Equation (A11) can be rewritten in the following form:

$$T = \frac{3}{2}\,\frac{p\,M}{\sigma\,L_s\,L_r}\,\varphi_s\,\varphi_r\,\cos\gamma. \tag{8}$$

At any instant, the torque is proportional to the stator flux magnitude, the rotor flux magnitude and the cosine of the angle γ (see Fig. 3).

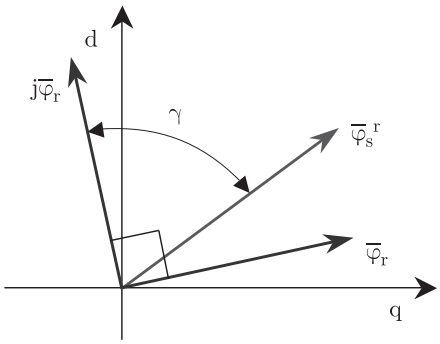

Fig. 3. Stator and rotor flux vectors representation

In balanced sinusoidal steady-state condition the stator and rotor fluxes rotate at constant angular speed $\omega_r = \omega_s - \omega$ in a rotor reference frame, which depends on the operating conditions. The angle γ maintains a constant value, which depends on the operating conditions too. In this way the produced torque is constant.

Starting from this condition, it is possible to analyze the effect produced from of a sudden variation of the angular speed of the stator flux space vector.

Taking (7) and (8) into account leads to the following results:

i) if $\bar{\varphi}_s^r$ accelerate, then γ decreases and the torque increases;

ii) if $\bar{\varphi}_s^r$ decelerate, then γ increases and the torque decreases.

The angular speed of the stator flux can be modified, in each cycle period, by an opportune choice of the inverter configuration. The tangential component of the applied voltage

vector determines the instantaneous angular speed of the stator flux in a stator reference frame.

The effect on the flux magnitude of a particular voltage vector depends on the position of the flux within the sector.

The effect on the torque of a particular voltage vector depends on the position of the flux within the sector and the rotor angular speed. This particular behaviour will be emphasized in Section 8.

4. DTC scheme

On the basis of the results obtained in previous Sections a basic control scheme for IM drive can be derived, which is shown in Fig. 4.

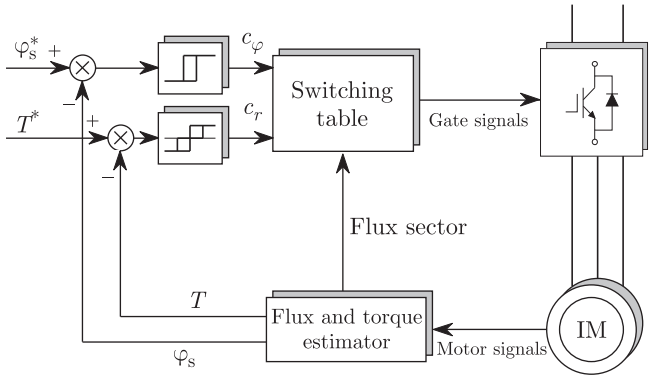

Fig. 4. Basic DTC scheme

In that scheme the error between the estimated torque T and the reference torque T^* is the input of a three level hysteresis comparator, whereas the error between the estimated stator flux magnitude φ_S and the reference stator flux magnitude φ_S^* is the input of a two level hysteresis comparator. The selection of the appropriate voltage vector is based on a switching table. The estimated torque in Fig. 4 can be determined by means of (A10). The stator flux, instead, is calculated by means of a suitable flux observer, that will be analyzed in details in Section 10.

5. Switching table

The use of a particular voltage vector selection strategy and the amplitudes of flux and torque hysteresis bands affect the performance of the drive.

On the basis of the previous results it is now possible to define the criteria for the selection of the voltage vector at any sampling instant. The results can be represented in a table that becomes the "Switching Table" of the DTC algorithm. As an example, with reference to the control scheme of Fig. 4, the following criteria can be adopted.

Comparator output	Selected VSI configuration
$c_\varphi = +1$	radial positive
$c_\varphi = -1$	radial negative
$c_T = +1$	tangential positive
$c_T = 0$	null
$c_T = -1$	tangential negative

The basic switching table, obtained from previous criteria, can be written in compact form introducing the parameter K that represents the number of the stator flux sector, as shown in Table 1. The choice of the null configuration (0 or 7) is based on the minimization of the inverter mean switching frequency.

Table 1
Switching table for a three level hysteresis torque comparator

c_φ	c_T		
	1	0	1
+1	k + 1	0 or 7	k-1
–1	k + 2	0 or 7	k-2

6. Switching strategies

For a prefixed switching strategy, the drive behaviour, in terms of torque and current ripple, switching frequency and torque response, is quite different at low and high speed [12,19]. In this Section a detailed discussion of some possible voltage vector selection criteria is carried out.

Table 2 summarizes the combined action of each inverter voltage space vector on both the stator flux amplitude and the motor torque. In the table, a single arrow means a small variation, whereas two arrows mean a larger variation. As can be seen, an increment of torque (↑) is obtained by applying the space vectors V_{k+1} and V_{k+2}, irrespective of the motor speed direction. Conversely, a decrement of torque (↓) is obtained by applying V_{k-1} or V_{k-2}. The space vectors V_k, V_{k+3} and the zero voltage space vectors modify the torque in accordance with the motor speed direction as specified in Table 2.

Table 2
Stator flux and torque variations due to the applied inverter voltage space vectors

	V_{k+1}	V_{k-1}	V_k	V_{k+1}	V_{k+2}	V_{k+3}	$V_0 V_7$
φ_S	↓	↑	↑↑	↑	↓	↓↓	↑↓
$T(\omega > 0)$	↓↓	↓↓	↓	↑	↑	↓	↓
$T(\omega < 0)$	↓	↓	↑	↑↑	↑↑	↑	↑

With hysteresis controllers having a two level output, there are four conditions regarding the stator flux and the motor torque voltage demands. For each condition it can be found at least one inverter voltage space vector that acts in the way of reducing the error signals. This demonstrates that a voltage inverter is able to regulate in a direct manner the stator flux amplitude and the motor torque of an IM or to force them so as to track any reference.

Table 3
Switching solutions

	T⇑ φ_s ⇑	T⇑ φ_s ⇓	T⇓ φ_s ⇑	T⇓ φ_s ⇓
ST-A	V_{k+1}	V_{k+2}	V_0, V_7	V_0, V_7
ST-B	V_{k+1}	V_{k+2}	V_k	V_0, V_7
ST-C	V_{k+1}	V_{k+2}	V_k	V_{k+3}
ST-D	V_{k+1}	V_{k+2}	V_{k-1}	V_{k-2}

Several switching solutions can be employed to control the torque according to whether the stator flux has to be reduced or increased. Each solution influences the drive behaviour in terms of torque and current ripple, switching frequency, and two- or four-quadrant operation capability. Assuming a two

level hysteresis comparator, four switching solutions are given in Table 3. Upon each solution, a Switching Table (ST) can be built and implemented in the block of Fig. 4. The ST inputs are the two-level demands of stator flux and torque, and the stator flux sector, whilst the ST output is the inverter voltage space vector for the motor.

Depending on the ST adopted, different behaviour of the drive are obtained. As an example, Fig. 5 reports the torque responses to a pulse in the reference torque from 18 to – 18 Nm for 8.8 ms, as obtained from an experimental prototype with ST-A and ST-D [12]. The motor under test is a 4 kW, 220 V, 50 Hz, 4 pole standard IM, with a large inertia load so as to keep its speed practically constant during the torque pulse. The results clearly document the influence of both ST and the working speed on the torque response. In particular, the response is sluggish at low speed when the zero space vectors are utilized, i.e. with ST-A, while it is quick with ST-D. On the contrary, at high speed the torque response is quick and almost identical with the two STs. This explains why ST-D is convenient for four-quadrant operation while ST-A (as well as ST-B, ST-C) is suitable for two-quadrant operation.

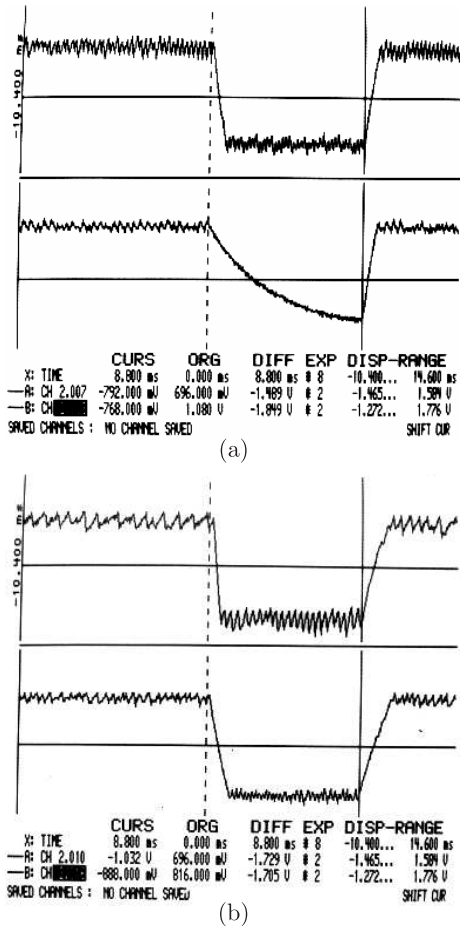

Fig. 5. Torque response to a 8.8 ms pulse in the reference from +18 to – 18 Nm, top trace: ST-D; bottom trace: ST-A, (a) motor speed: 20 rad/s, (b) motor speed: 100 rad/s

To give a theoretical assessment to the torque responses in Fig. 5, the relationship between the incremental motor torque and the corresponding voltage applied to the stator will be analyzed in Section 8.

7. Influence of the hysteresis band amplitudes

The amplitudes of the hysteresis bands have a significant impact on the drive performance [10]. In particular, the harmonic current distortion, the average inverter switching frequency, the torque pulsation and the drive losses are strongly influenced by the amplitudes of these bands.

In digital implementation schemes too small values of the bands amplitude lead to a high value of the inverter switching frequency, without reducing the ripple amplitude. In fact, the minimum value of the ripple amplitude depends on the minimum variation of torque and flux achievable in a cycle period that, in turn, depends on the values of V_c and T_c.

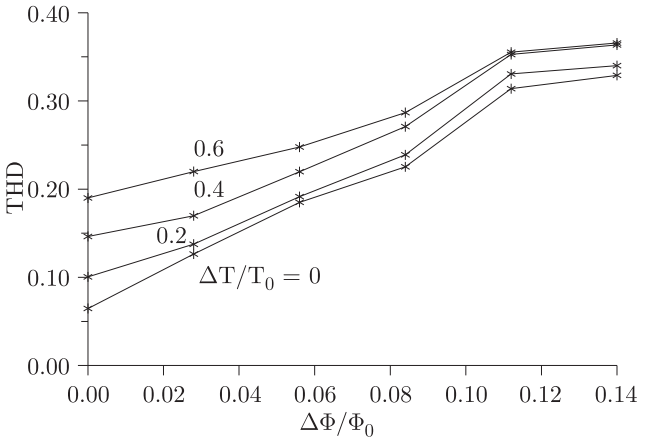

Fig. 6. THD factor as a function of the hysteresis band amplitudes, ST-A

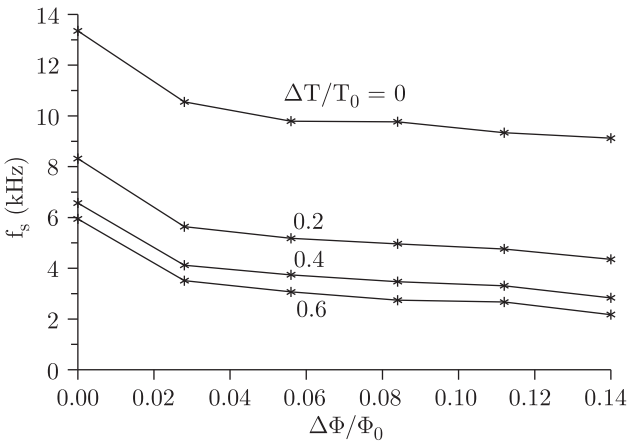

Fig. 7. Average inverter switching frequency as a function of the hysteresis band amplitudes, ST-A

As an example, Figs. 6 and 7 give the THD factor of the stator current and the average switching frequency of the inverter, respectively, as a function of the band amplitudes. The results show that the hysteresis band of the stator flux mainly influences the stator current THD and hence the associated copper losses, giving rise a significant increase of THD when enlarging its amplitude. On the other hand, the hysteresis band of the

torque mainly influences the switching frequency and hence the associated switching losses. In case that the motor parameters and the inverter switching characteristics are known, a possible criterion in designing the band amplitudes consists in minimizing the sum of the harmonic copper losses and the switching losses.

8. Motor torque-stator voltage relationship

In order to deeply analyze the basic DTC principles it is possible to determine the analytical relationships between the applied voltage vector and the corresponding torque and flux variations.

For this purpose reference is made to the IM equations in a stationary reference frame, written in the state-space form

$$\begin{bmatrix} \frac{d\bar{\varphi}_s}{dt} \\ \frac{d\bar{\varphi}_r^s}{dt} \end{bmatrix} = \begin{bmatrix} -\frac{R_s}{\sigma L_s} & \frac{R_s M}{\sigma L_s L_r} \\ \frac{R_r M}{\sigma L_s L_r} & j\omega - \frac{R_r}{\sigma L_r} \end{bmatrix} \begin{bmatrix} \bar{\varphi}_s \\ \bar{\varphi}_r^s \end{bmatrix} + \begin{bmatrix} 1 \\ 0 \end{bmatrix} \bar{v}_s. \quad (9)$$

Equations (9) can be discretized by means of the small-signal analysis. For small values of $T_c = t_{k+1} - t_k$ the stator and rotor flux space vectors at t_{k+1} can be expressed as

$$\bar{\varphi}_{s_{k+1}} = \bar{\varphi}_{s_k} \left(1 - \frac{R_s}{\sigma L_s} T_c\right) + \bar{\varphi}_{r_k}^s \frac{R_s M}{\sigma L_s L_r} T_c + \bar{v}_{s_k} T_c \quad (10)$$

$$\bar{\varphi}_{r_{k+1}}^s = \bar{\varphi}_{r_k}^s \left[1 + \left(j\omega_k - \frac{R_r}{\sigma L_r}\right) T_c\right] + \bar{\varphi}_{s_k} \frac{r_r M}{\sigma L_s L_r} T_c. \quad (11)$$

Equations (10) and (11) are the discrete-time equations of an IM. Note that in (11) the stator voltage $\bar{v}_{s_k}$ does not appear explicitly, meaning that $\bar{v}_{s_k}$ acts on the rotor through the stator flux.

Furthermore, the electromagnetic torque at t_{k+1} is given by

$$T_{k+1} = \frac{3}{2} p \frac{M}{\sigma L_s L_r} \left(\bar{\varphi}_{s_{k+1}} \cdot j\bar{\varphi}_{r_{k+1}}^s\right). \quad (12)$$

Substituting (10) and (11) into (12) and neglecting the terms proportional to the square of T_c, the torque at t_{k+1} can be expressed as

$$T_{k+1} = T_k + \Delta T_{k_1} + \Delta T_{k_2} \quad (13)$$

where

$$\Delta T_{k_1} = -T_k \left(\frac{R_s}{L_s} + \frac{R_r}{L_r}\right) \frac{T_c}{\sigma} \quad (14)$$

$$\Delta T_{k_2} = p \frac{M}{\sigma L_s L_r} \left[\left(\bar{v}_{s_k} - j\omega_k \bar{\varphi}_{s_k}\right) \cdot j\bar{\varphi}_{r_k}^s\right] T_c. \quad (15)$$

The term ΔT_{k_1} has opposite sign of T_k and then reduces the torque; its value is proportional to the stator and rotor resistances and to the torque at t_k and is independent of $\bar{v}_{s_k}^s$ and the motor speed.

The term ΔT_{k_2} is due to the stator voltage and depends on the operating conditions (i.e. the motor speed and the torque angle between $\bar{\varphi}_{s_k}$ and $\bar{\varphi}_{r_k}^s$). This relationship is illustrated by the diagram of Fig. 8 where the stator flux $\bar{\varphi}_{s_k}$ is assumed lying on the d-axis, the dashed lines are parallel to $\bar{\varphi}_{r_k}^s$ and that one crossing the q-axis at the ordinate $\omega_k \varphi_{s_k}$ is bold-faced. A graphical representation of $\Delta T_k = \Delta T_{k1} + \Delta T_{k2}$, useful to visualize the effects of the applied voltage vector on the motor torque, is drawn in Fig. 9 for zero motor speed and in Fig. 10 for the rated motor speed.

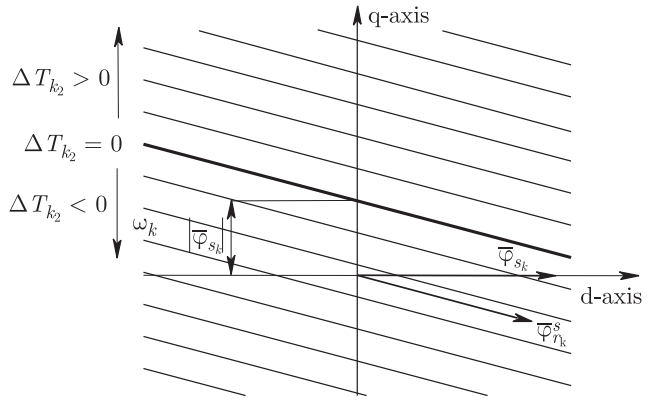

Fig. 8. Diagram of the torque variation ΔT_{k_2}

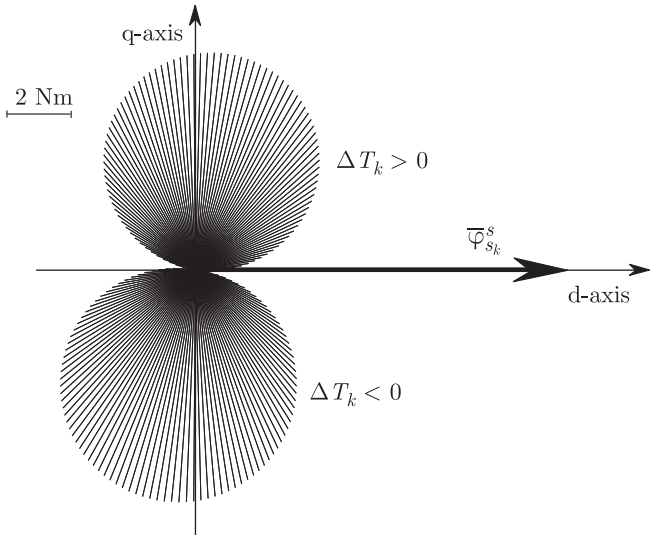

Fig. 9. Torque variations at zero speed (rated torque)

These figures report the torque variation ΔT_k produced by a stator voltage space vector of constant amplitude and for several values of its displacement with respect to the stator flux. The segments have a length proportional to the torque variation and the same direction as the stator voltage space vector. The ones in the upper part of the figures represent positive variations of the torque while those in the lower part represent negative variations.

Figures 9 and 10 point out the influence of the motor speed. In particular they show that along some directions the same stator voltage produces positive variations of motor torque at low speed and negative variations at high speed. This effect should be taken into account when defining ST and can lead to the use of a speed-dependent ST (ST-A at high speeds and ST-D at low speeds). The advantages of this solution are a better torque response over the whole speed range and a reduction in the torque ripple.

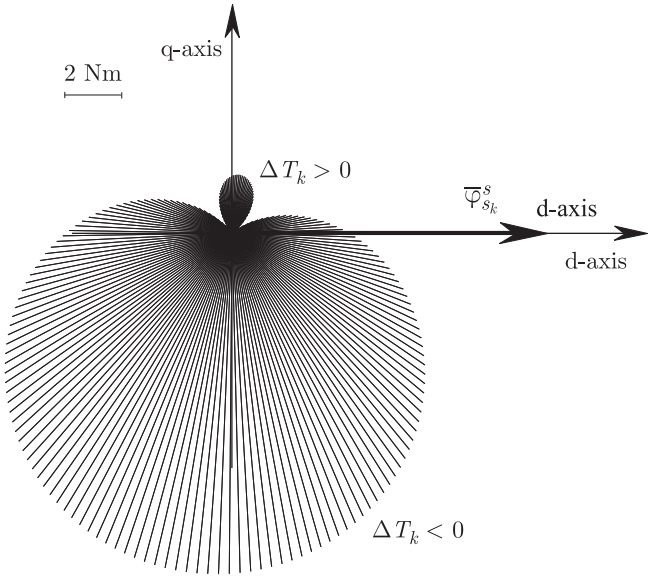

Fig. 10. Torque variations at rated speed (rated torque)

9. DSC scheme

In high power electrical drives the semiconductor devices cannot be switched at high frequency. As a consequence, a precise control of both the stator flux amplitude and the motor torque is not achievable.

The DSC scheme is aimed at minimizing the inverter switchings in each supply period to the detriment of the control of the stator flux amplitude [4–6]. As a matter of fact, this strategy commands the stator flux space vector every sixty degrees of the supply period so as to move it along an hexagon. The motor torque, instead, is controlled in a precise way by means of a hysteresis controller like in the DTC scheme.

The block diagram of an IM drive controlled with DSC is drawn in Fig. 11.

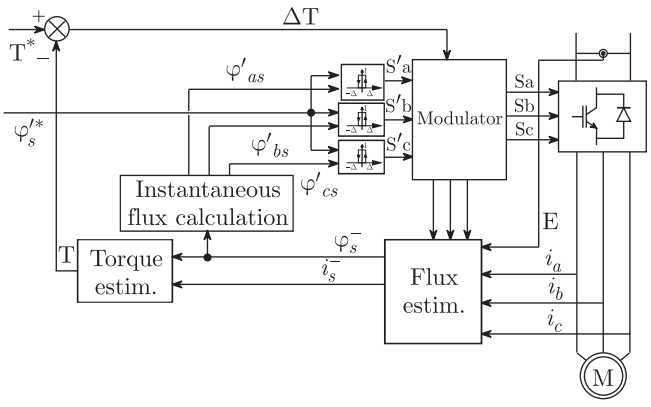

Fig. 11. DSC IM drive block diagram

The flux estimator allows calculating the instantaneous values of the stator phase fluxes $\varphi_{as}, \varphi_{bs}, \varphi_{cs}$ and the motor torque. The fluxes are calculated and compared with the reference flux. The results of the comparison provide the switch signals corresponding to a given voltage space vector. On the basis of the torque error, the modulator selects the active voltage vector or the zero voltage vector in order to keep the torque within the hysteresis band.

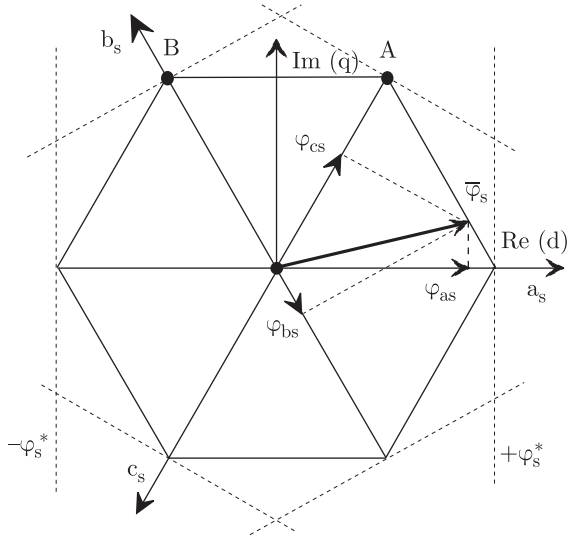

Fig. 12. DSC principle

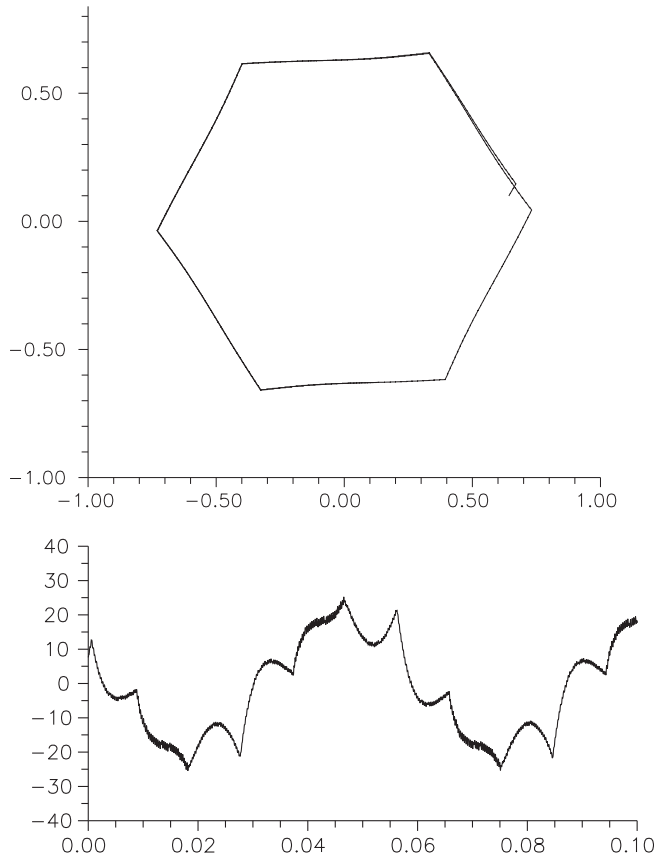

Fig. 13. Stator flux space vector trajectory and current waveform of a DTC scheme with $\Delta\varphi_s = 0.14\varphi_s^*$

According to the principle of operation outlined in Fig. 12 and for a counterclockwise rotation of stator flux, before point A is reached, the active voltage vector utilised is $\bar{V}_3$. After point

A the active voltage vector utilised is $\bar{V}_4$. The basic rule is that when a phase flux exceeds the lower limit the corresponding switch state S is set to 1; when a phase flux exceeds the upper limit the corresponding switch state S is set to 0. This control method is no longer valid when the reference flux is changed. It is possible to verify that in this case the trajectory described by the flux leaves the hexagon. However, with an opportune implementation, it is possible to prevent this occurrence.

It can be noted that the behaviour of a DSC scheme can be reproduced by a DTC scheme with an opportune value of the flux hysteresis band $\Delta\varphi_s$. As an example, Fig. 13 shows the trajectory of the stator flux space vector and the stator current waveform as obtained from a DTC drive with $\Delta\varphi_s = 0.14\varphi_s^*$.

10. Improved DTC schemes

In this section some improvements to basic DTC scheme that allow increasing the pull-out torque, to reduce the sensitivity to parameter deviation and to obtain a constant switching frequency operation, will be analyzed. Many efforts have been made in order to reduce the main drawbacks of DTC [19–28].

10.1. Rotor flux reference. A new DTC scheme can be developed assuming torque and rotor flux as references [9]. In this way, the highest pull-out torque is obtained and it is possible to combine the advantages of rotor flux orientation and stator flux control. The strategy adopted needs neither the rotor resistance of the machine nor the coordinate transformation based on the rotor flux position, leading to a high performance drive using a simple control scheme.

From the IM equations, the following expressions of the electromagnetic torque can be found at steady state as a function of either the rotor flux or the stator flux:

$$T = \frac{3}{2} p \omega_r \frac{\varphi_r^2}{R_r} \tag{16}$$

$$T = \frac{3}{2} p \left(\frac{M}{L_s}\right)^2 \frac{R_r \omega_r}{R_r^2 + \omega_r^2 (\sigma L_r)^2} \varphi_s^2. \tag{17}$$

Note that (16) is valid also during transients. By (16)–(17), the torque characteristic of an IM under constant rotor flux operation increases linearly with ω_r, and the maximum torque is constrained by the maximum current allowable for the inverter. On the contrary, the torque characteristic under constant stator flux operation exhibits a maximum value at an angular slip speed which depends on the machine parameters. This suggests to control the amplitude of the rotor flux instead of that of the stator flux in order to increase the overload torque capability of a ST scheme [29].

From the IM equations, written in a reference frame synchronous with the rotor flux and aligned with the d-axis, the space vector of the stator flux can be expressed as [30].

$$\bar{\varphi}_s = \frac{L_s}{M} \left[(1 + s\sigma\tau_r)\, \varphi_r + j \frac{\sigma L_r}{\varphi_r} \frac{2}{3} \frac{T}{p} \right]. \tag{18}$$

Its amplitude furnishes the reference for the stator flux amplitude needed by a DTC scheme, as a function of the rotor flux and torque references. Under constant rotor flux operation, it becomes

$$\varphi_s^* = \frac{L_s}{M} \sqrt{(\varphi_r^*)^2 + \left(\frac{2}{3} \frac{\sigma L_r}{p}\right)^2 \left(\frac{T^*}{\varphi_r^*}\right)^2}. \tag{19}$$

To emphasize the high overload capability of a DTC 220V, 4 kW, 2-pole IM drive, with constant rotor flux, Fig. 14 shows the output torque and stator current magnitude for a step change in torque command from 50% to 300% of the rated motor torque. Figure 15 shows the stator and rotor flux loci during the same time interval.

As it is possible to see the rise time of the torque is about 3 ms and the rotor flux locus is a circle. The stator flux locus shows the increase in flux magnitude required to maintain the rotor flux magnitude fixed to the commanded value.

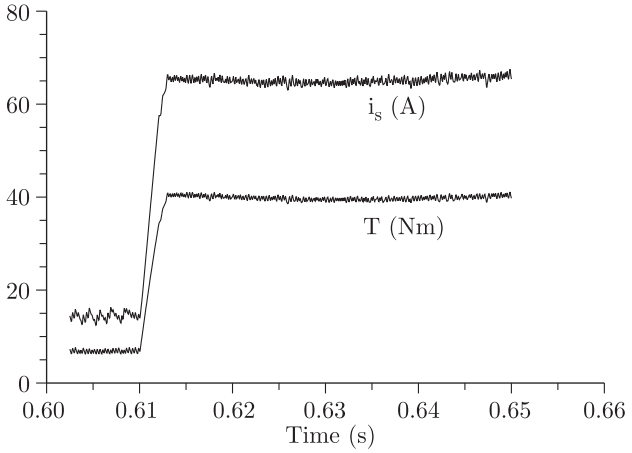

Fig. 14. Torque and current magnitude during torque step response

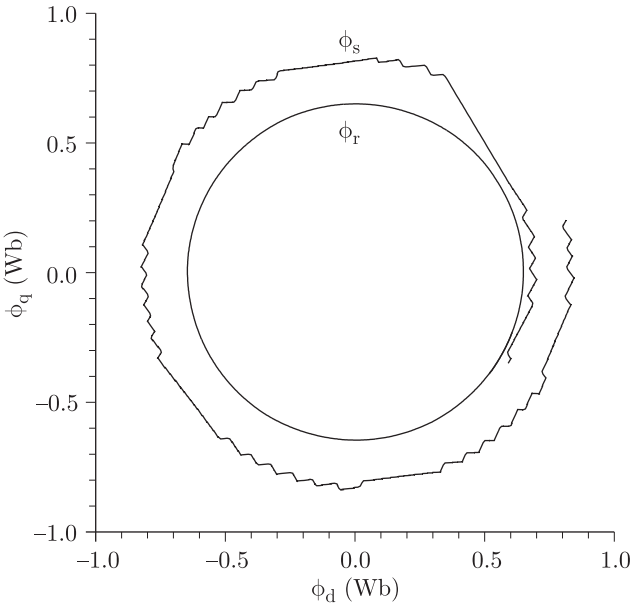

Fig. 15. Stator and rotor flux loci during torque step response

10.2. Improved stator flux estimator. In sensorless applications the stator flux is evaluated by stator voltages and currents. At low speed this estimation deteriorates owing to stator resistance variations and current sensor offsets, leading to undesired oscillations of the stator flux magnitude, torque oscillations and acoustic noise.

Some possible solutions are given by the use of high accuracy current sensors and on-line stator resistance estimation. However, these solutions increase cost and computational time without achieving sometimes the expected results.

To maintain good performance at low speed, improved flux estimators have been devised [19,24,25,31,32].

A possible solution is based on correcting the flux estimate on the basis of the rotor flux command. This flux estimator can be applied to both DTC and FOC schemes.

The stator flux can be determined integrating the following stator voltage equation:

$$\frac{d\bar{\varphi}_s^s}{dt} = \bar{v}_s^s - R_s\bar{i}_s^s + \frac{\left(\varphi_r^{s*}e^{j\theta} - \bar{\varphi}_r^s\right)}{\tau}. \tag{20}$$

where θ is the phase angle of the rotor flux vector, φ_r^{s*} is the reference magnitude of the rotor flux vector, and τ is the observer time constant.

The rotor flux can be estimated as follows

$$\bar{\varphi}_r^s = \frac{L_r}{M}\left(\bar{\varphi}_s^s - \sigma L_s\bar{i}_s^s\right) \tag{21}$$

whereas θ can be derived from (21) as follows

$$\theta = \arg\bar{\varphi}_r^s = \arg\left(\bar{\varphi}_s^s - \sigma L_s\bar{i}_s^s\right). \tag{22}$$

It is evident from (20) that the estimation of the stator flux vector can be affected by stator resistance mismatch, sensor offsets and the inverter non-linearity (inverter dead-times, voltage drop on the conducting switches, etc.). However, at high speed the estimation error is lower than that at low speed, because the input voltage becomes the most relevant term in the second member of (20). The estimation error on the phase angle θ depends on the stator flux estimation error, the mismatch on the leakage inductance σLs and the offset of the current sensors. The leakage inductance shows moderate variations with the stator currents and it will be assumed practically constant.

In conclusion, the rotor flux observer depends on three machine parameters, namely R_s, σL_s, and L_r/M but the effects of this dependence can be considered negligible in the high speed range. In the low speed range, instead, the closed loop scheme of the flux observer can reduce the effect of the parameter and model mismatch, and sensor offsets.

The low-speed performance of the drive depends on the parameter τ. An appropriate value of τ greatly improves the dynamic robustness of the scheme. By selecting τ to be very large the filter approximate a pure integrator and the estimation at low speed becomes difficult. On the other hand, by selecting τ to be very small reduces the contribution of the rotor back-emf and the estimation at high speed becomes difficult. As a consequence, in drive systems operating in a wide speed range, good results can be achieved choosing a speed dependent value of τ.

A block diagram of a DTC IM drive with the improved stator flux estimator and the control of the rotor flux amplitude is drawn in Fig. 16. In order to emphasize the benefits of the improved stator flux estimator Fig. 17a) shows the system response to a step torque command from 0 to the rated torque.

It can be noted that using a pure integrator it is not possible to magnetize the machine if a zero torque command is applied. As a consequence, a slow torque increase is observed owing to the transient required to magnetize the machine when the torque command is applied. Fig. 17b) shows the results obtained when the improved flux estimator is used.

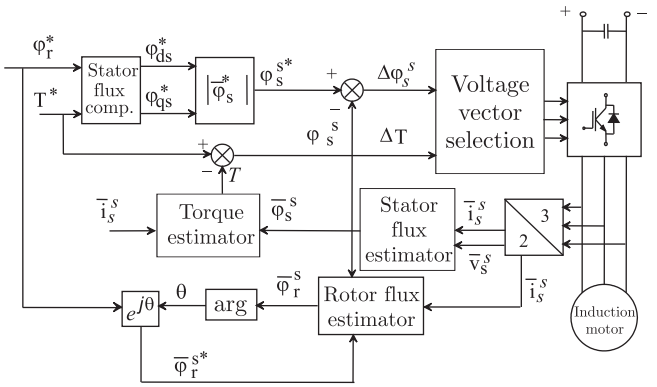

Fig. 16. Block diagram of a DTC scheme with improved stator flux estimator

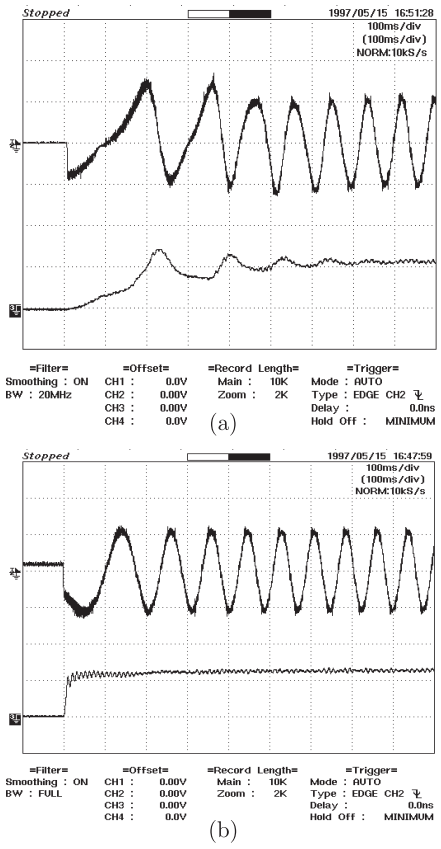

Fig. 17. Torque step response during the start-up, upper trace: phase current, 20 A/div, lower trace: measured torque, 20 Nm/div, (a) pure integrator, (b) improved flux estimator, $\tau = 0.01$ s

In this case, with zero torque command, the phase current assumes a constant value, corresponding to the magnetizing current. As the torque command is applied to the control system the output torque reaches the reference value in few milliseconds.

10.3. Constant switching frequency DTC schemes. In DTC schemes, the presence of hysteresis controllers for flux and torque determines variable switching frequency operation for the voltage source inverter. This problem can be overcome by different methods[33,34].

A solution based on Stator Flux Vector Control (SFVC) scheme has been proposed [30,35–37]. This scheme, presented in Fig. 18, may be considered as a development of the basic DTC scheme with the aim of improving the drive performance. The input commands are the torque and the rotor flux, whereas the control variables are the stator flux components, according to (18). It should be noted that the real and imaginary parts of (18) are quite similar to the corresponding equations of the traditional field oriented control based on stator currents.

The principle of operation is based on driving the stator flux vector toward the corresponding reference vector defined by the input commands. This action is carried out by the Space-Vector Modulation (SVM) technique, which applies a suitable voltage vector to the machine in order to compensate the stator flux vector error. In this way it is possible to operate the induction motor drive with a constant switching frequency.

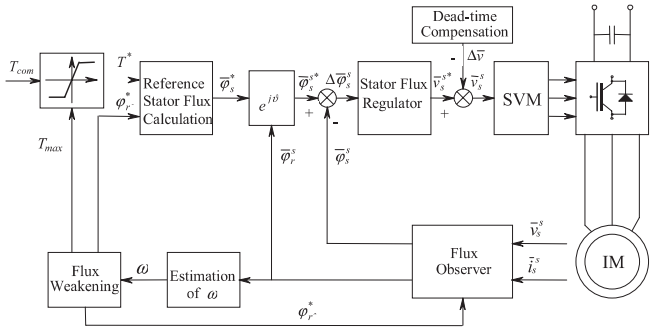

Fig. 18. Block diagram of the scheme based on Stator Flux Vector Control

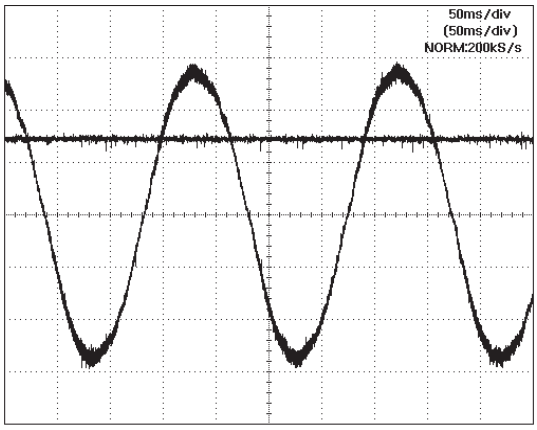

Fig. 19. Motor current (10 A/div) and estimated torque (18 Nm/div) in the locked rotor test with rated torque and flux commands (50 ms/div)

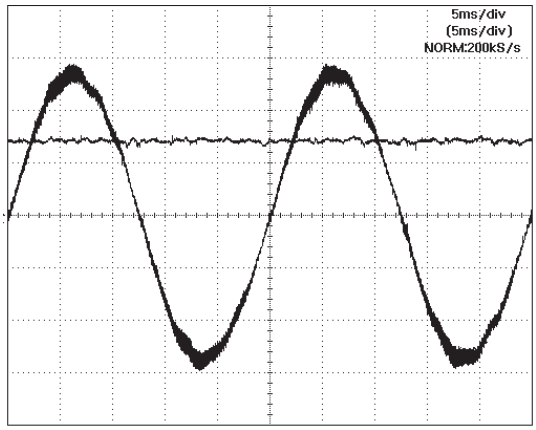

Fig. 20. Motor current (10 A/div) and estimated torque (18 Nm/div) in steady state conditions at rated current, 1120 rpm (5 ms/div)

10.4. Stator flux regulator. The flux regulator determines the voltage vector, which has to be applied to the motor in order to obtain, at any instant, a stator flux vector equal to its reference value $\bar{\varphi}_s^*$. This can be properly obtained by using a regulator in which the input variable is the difference between the reference and the estimated flux vectors

$$\Delta\bar{\varphi}_s = \bar{\varphi}_s^* - \bar{\varphi}_s. \tag{23}$$

The flux regulator equation can be expressed as follows

$$\bar{v}_s^* = R_s\bar{i}_s + j\omega_s\bar{\varphi}_s + K_p\Delta\bar{\varphi}_s. \tag{24}$$

This equation shows that the flux regulator behaves as a proportional controller, with some additional terms compensating the stator back emf and the stator resistance voltage drop, according to (A6). In (24) K_p represents the gain of the regulator.

10.5. Experimental results. The control algorithm has been implemented on a low cost, fixed point DSP, which performs the calculations and produces the PWM signals. Dead time compensation has been included in the control algorithm.

Several experimental tests have been carried out and good results have been achieved in both steady state and transient operating conditions. Figures 19 and 20 show the motor current and the estimated torque in the locked rotor tests and in steady-state conditions, respectively. As it can be seen, the motor current is practically sinusoidal. The estimated torque matches the measured as well as the reference torque.

10.6. Sensitivity investigation of a speed sensorless induction motor drive based on stator flux vector control. Reliable operation of SFVC schemes depends on how closely the estimations of the stator flux and motor torque approximate their actual values, particularly in the low speed range.

In order to evaluate the performance of the drive and its sensitivity to stator parameter deviations and current sensor offsets, a detailed analysis is necessary, considering the equations of the whole system. In particular, the equations of the

machine, the control system and the flux estimator can be developed through the linearization at a steady state operating point. Then, the relationships linking the stator resistance deviations and the current sensor offsets with the rotor flux may be determined. In this way, both the control system stability and the effects of parameter sensitivity on the drive performance can be examined.

To estimate the sensitivity of the control system, the stator resistance and the measured stator current are related to the actual values by

$$\hat{R}_s = R_s + \Delta R_s \qquad \hat{\bar{i}}_s = \bar{i}_s + \Delta \bar{i}_s. \tag{25}$$

The system equations have been linearized around the steady-state operating point of the motor drive considered without parameter mismatch.

$$\begin{bmatrix} \frac{d}{dt}\Delta\varphi_{rd} \\ \frac{d}{dt}\Delta\varphi_{rq} \\ \frac{d}{dt}\Delta\hat{\varphi}_r \end{bmatrix} = [A] \begin{bmatrix} \Delta\varphi_{rd} \\ \Delta\varphi_{rq} \\ \Delta\tilde{\varphi}_r \end{bmatrix} + [B] \begin{bmatrix} \Delta R_s \\ \Delta i_{sd} \\ \Delta i_{sq} \end{bmatrix} \tag{26}$$

where

$$[A] = \begin{bmatrix} -\frac{1}{\tau_r} & \hat{\omega}_{s_0} - \omega_0 & -\frac{M^2}{\sigma L_s L_r \tau_r} \\ -\hat{\omega}_{s_0} & 0 & \hat{\omega}_{s_0} \\ -\frac{1}{\tau_r} & -\omega_0 & -\frac{1}{\tau} - \frac{M^2}{\sigma L_s L_r \tau_r} \end{bmatrix} \tag{27}$$

$$[B] = \begin{bmatrix} 0 & -\frac{M}{\tau_r}\cos\hat{\theta}^s_{r_0} & -\frac{M}{\tau_r}\sin\hat{\theta}^s_{r_0} \\ \frac{L_r^2}{M^2}\frac{T_0^*}{p\varphi^*_{r_0}} & -\frac{L_r R_s}{M}\sin\hat{\theta}^s_{r_0} & \frac{L_r R_s}{M}\cos\hat{\theta}^s_{r_0} \\ -\frac{L_r}{M^2}\varphi^*_{r_0} & -\left(\frac{M}{\tau_r}+\frac{L_r R_s}{M}\right)\cos\hat{\theta}^s_{r_0} & -\left(\frac{M}{\tau_r}+\frac{L_r R_s}{M}\right)\sin\hat{\theta}^s_{r_0} \end{bmatrix} \tag{28}$$

where $\hat{\theta}^s_{r_0}$ is the argument of the estimated rotor flux.

10.7. Stability analysis. The stability analysis can be carried out determining the eigenvalues of matrix [A] [37].

The results show that in the case of a pure integration to estimate the flux leads to limit operating conditions for the system stability. When the flux estimation is performed by the "improved estimator" the system stability can be investigated by solving the characteristic equation of matrix $[A]$. As an example, Fig. 21 shows the contour lines of the surface representing the real part of the dominant pole as function of and τ. The figure is related to a slip angular frequency of 5 rad/s. In Fig. 21 the dashed area represents instability regions. It can be noted that for positive values of ω_s the system is always stable. For negative values of ω_s the instability region can be avoided choosing a suitable value of τ.

From the analysis carried out it can be noted that the stability of the control system is increased using the improved estimator.

10.8. Sensitivity analysis. The system of equations (26) can also be used to investigate the sensitivity of the control system. In particular, solving (26) in steady-state conditions yields the relationships linking the stator resistance deviation and the current measurement error with the variables $\Delta\varphi_{rd}$, $\Delta\varphi_{rq}$ and $\Delta\hat{\varphi}_r$.

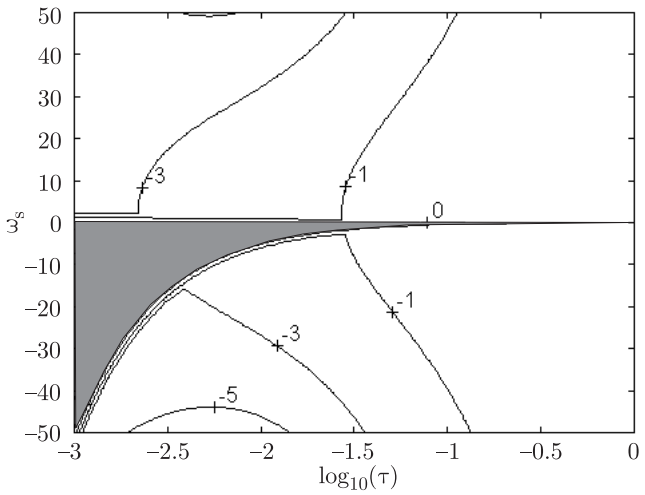

Fig. 21. Contour lines of the surface representing the real part of the dominant pole for a slip angular frequency of 5 rad/s

Stator resistance error. Considering a stator resistance deviation it can be verified that the rotor flux error is practically independent of the value of τ (Fig. 22). However, the use of the improved estimator with low values of τ increases the system stability. In fact, using the improved flux estimator, the overestimation of R_s leads to a steady state error of the rotor flux magnitude equal to that predicted by the theoretical approach, as shown in Fig. 23.

On the contrary, the basic flux estimator exhibits an oscillatory response with increasing amplitude. This behavior has been observed also during experimental tests with an evident increase of the noise level and the generation of a pulsating torque.

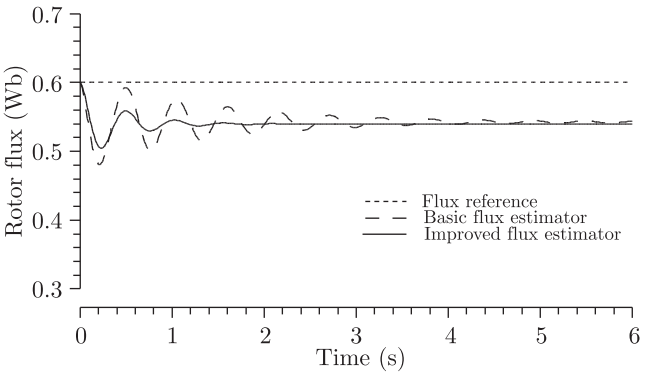

Fig. 22. Rotor flux error due to 10% underestimation of the stator resistance, $\omega = 1$ rad/s, $\tau = 0.01$ s, T = 100% rated torque

Current measurement error. Considering a current measurement offset, it can be verified that large values of τ, which transform the improved estimator in a pure integrator, increase the steady-state error in the rotor flux magnitude.

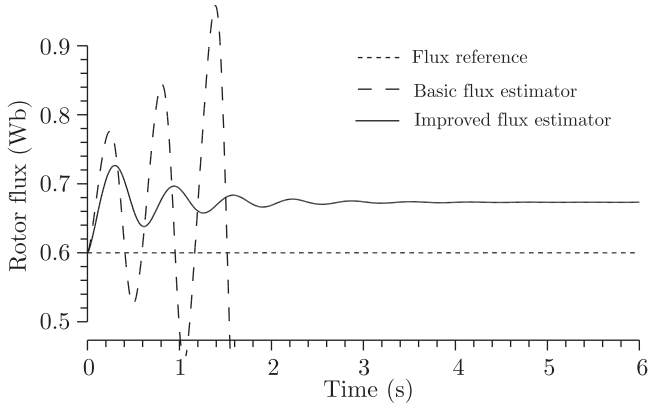

Fig. 23. Rotor flux error due to 10% overestimation of the stator resistance, $\omega = 1$ rad/s, $\tau = 0.01$ s, T = 100% rated torque

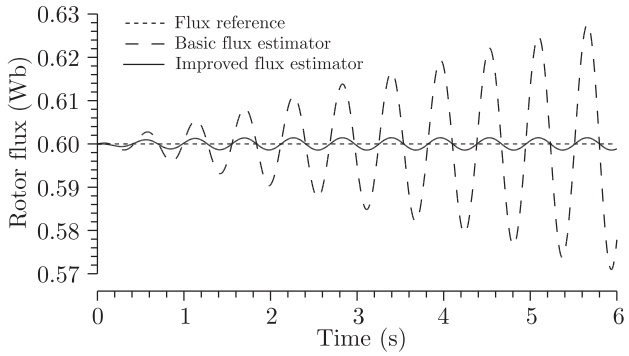

Fig. 24. Rotor flux error due to 0.01 A offset, $\omega = 1$ rad/s, $\tau = 0.01$ s,T = 100% rated torque

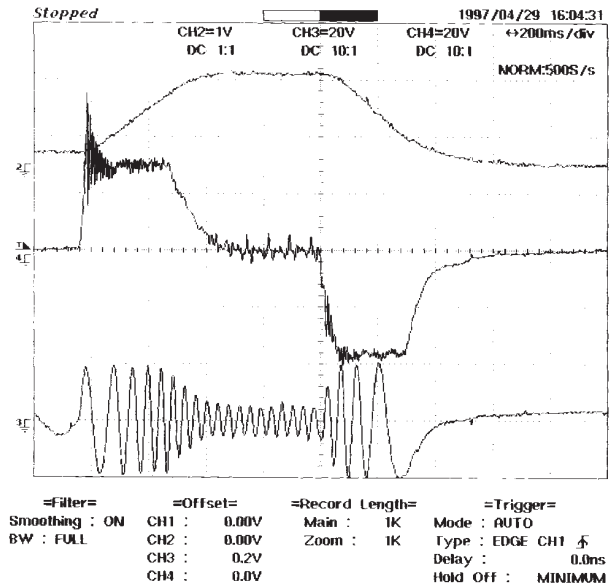

Fig. 25. Transient response of the drive system, top trace: rotor angular speed, middle trace: measured torque, bottom trace: line current, 2 s total acquisition time $\Delta R_s = -10\%$, $\omega = 0$ rad/s, $\tau = 0.01$ s

Figure 24 illustrates the rotor flux error obtained in presence of a current sensor offset. With the improved flux estimator the rotor flux magnitude oscillates around the reference value and both the amplitude and the frequency of the oscillation are equal to that predicted by the theory.

The basic flux estimator shows an oscillation with the same frequency of that obtained by the improved estimator, but with increasing amplitude. This oscillation in turn determines torque pulsations as it has been verified by experimental tests.

The results obtained show that in all cases the improved estimator leads to stable operating conditions, even if the flux level is not properly maintained and the torque is not the commanded value.

10.9. Experimental results. Figure 25 illustrates the experimental results when a machine is firstly accelerated from 50 rpm to 220 rpm, then decelerated to 0 rpm to show the drive behaviour during regenerative braking.

11. Discrete space vector modulation for DTC induction motor drives

The possibility to compensate, at each cycle period, the torque and flux errors is strongly dependent on the number of available voltage vectors.

A high number of voltage vectors can be generated using non-traditional power circuit topology as proposed in literature [3,38–40].

In effect, the number of voltage vectors can be increased using a standard VSI topology and introducing a simplified space vector modulation technique [41–44].

According to the principle of operation, new voltage vectors can be synthesized by applying, at each cycle period, several voltage vectors for prefixed time intervals. In this way a sort of Discrete Space Vector Modulation (DSVM) is employed which requires only a small increase of the computational time. The number of the voltage vectors that can be generated is directly related to the numbers of time intervals by which the cycle period is subdivided. It has been verified that subdividing the cycle period in three equal time intervals leads to a substantial reduction of torque and current ripple without the need of too complex switching tables.

In basic DTC schemes, 5 voltage vectors are usually employed to compensate flux and torque errors. Using the DSVM technique, with three equal time intervals, 19 voltage vectors can be used, as represented in Fig. 26.

As an example, the label “332” denotes the voltage vector which is synthesized by using the voltage space vectors V_3, V_3 and V_2 , each one applied for one third of the cycle period.

The voltage vector selection strategy should be defined using all the 19 voltage vectors on the basis of the criteria discussed in the Section 8. In particular it has been verified a large influence exerted by the dynamic emf $\omega_k \varphi_{s_k}$. So this quantity together with the actual outputs of flux and torque comparators must be assumed as input variable to the switching tables.

The results of the analysis can be summarized in seven switching tables for the stator flux lying in a given sector.

The first switching table is valid for low speed operation, the second for medium speed and the last two for high speed.

The speed ranges are defined with reference to the value assumed by the dynamic emf $\omega_k \varphi_{s_k}$, as represented in Fig. 27.

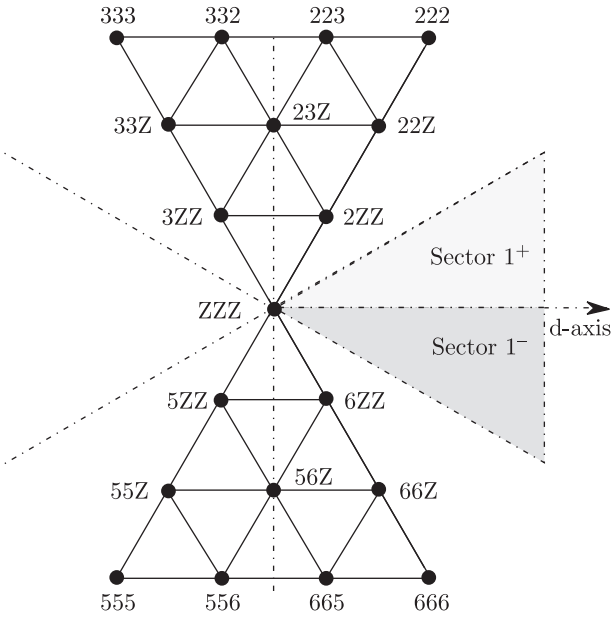

Fig. 26. Voltage vectors obtained by using DSVM with three equal time intervals per cycle period

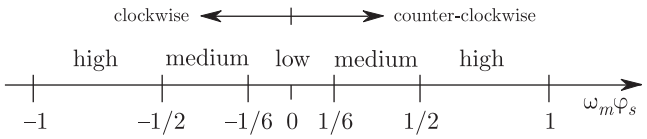

Fig. 27. Speed range subdivision, p.u. of the rated voltage

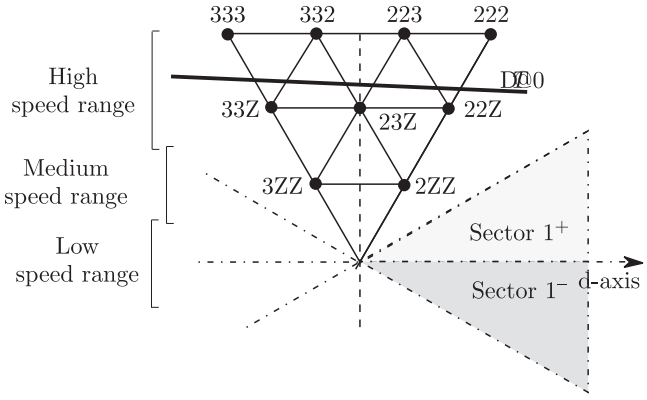

Fig. 28. Representation of the voltage vectors used by the DSVM technique in the high speed range

In the high speed range two switching tables have been defined, each one valid for half a sector (1^+ and 1^-). This means that the argument of the stator flux vector has to be estimated with a resolution of $\pi/6$, corresponding to a 12-sector angular representation. The two switching tables are necessary at high speed to fully utilize the available voltage vectors.

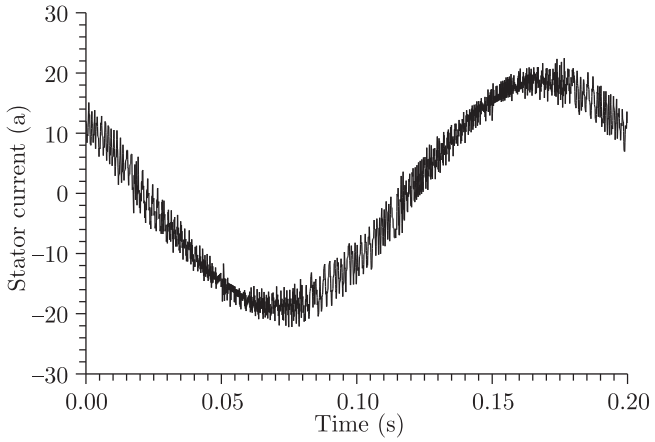

Fig. 29. Basic DTC, $\Delta t = 80$ µs, $B_T = 5\%$, $B_\varphi = 2\%$, $f_s = 2450$ Hz, 100 rpm

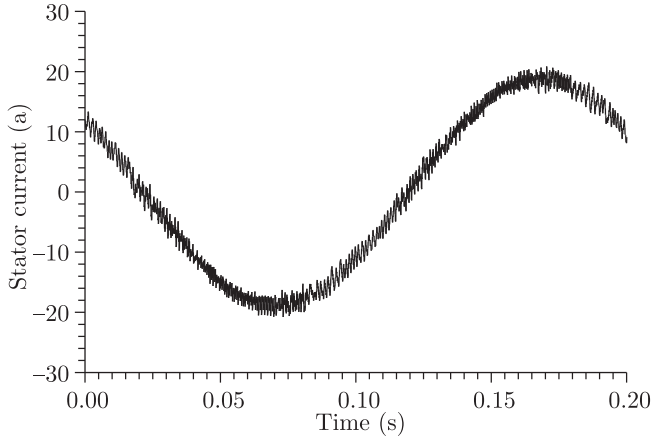

Fig. 30. DSVM, $\Delta t = 160$ µs, $B_T = 2.5\%$, $B_\varphi = 1\%$, $f_s = 2450$ Hz, 100 rpm

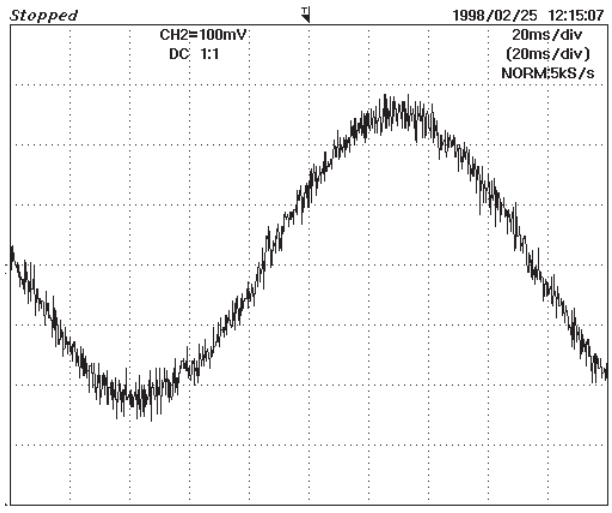

Fig. 31. Measured motor current (8 A/div)

In order to explain how the synthesized voltage vectors are selected at high speed, we assume for the machine a counter-clockwise rotation and a torque increase demand. In this case

the bold-faced line of Fig. 8, is located in the high speed range of Fig. 28. Then 4 voltage vectors can be employed, i.e. "333", "332", "223" and "222". Depending on whether the flux has to be reduced or increased, the first two vectors or the last two vectors respectively should be selected. For the last step we have to verify the position of the flux vector. If the flux is in sector 1^+ the vector "333" is selected, while with the flux in sector 1^- it is opportune to select "332".

The speed value required to choose the different switching tables is not critical so, in sensorless applications, the speed range can be selected from the estimation of the stator angular frequency.

Figures 29 and 30 show a comparison of the steady state behaviour obtained using the basic DTC scheme and the new DSVM scheme. The machine is running at 100 rpm. As it is possible to see an appreciable reduction of current ripple has been obtained using the DSVM technique. It should be noted that the performance improvement has been achieved with a mean switching frequency (f_s) practically equal to that of basic DTC scheme.

Figure 31 shows the experimental results obtained with a rotor speed of 100 rpm and rated torque command. The performance of the DSVM drive system is satisfactory, showing an acceptable level of torque and current ripple and a reduction of the acoustic noise with respect to that of basic DTC scheme, particularly in the low speed range.

12. DTC in the high speed range

In flux controlled drives the selection of the flux reference and of the base speed is very critical, particularly with reference to the dynamic performance [45–50].

A very interesting effort toward a robust flux weakening strategy has been proposed in [51]. However, that method requires large computing time and needs the tuning of several PI regulators.

In DTC induction motor drives, a new strategy for the flux weakening operation, suitable for electric vehicle applications, can be adopted [52]. The main features of the proposed flux weakening strategy include no dependency on machine parameters and smooth transition into and out of the flux weakening mode.

12.1. Basic equations. If the stator flux magnitude is assumed constant, from (17) it appears that the torque reaches its maximum value

$$T_M = k_T \phi_s^2 \tag{29}$$

for the following value of the rotor angular frequency

$$\omega_r = R_r / \sigma L_r. \tag{30}$$

where

$$k_T = \frac{3}{4} p \frac{M^2}{\sigma L_r L_s^2}. \tag{31}$$

The torque expression (29) emphasizes an intrinsic torque limit related to the value of the stator flux magnitude. Furthermore, the stator voltage equation, written in balanced sinusoidal steady-state conditions, leads to

$$\left|\bar{\phi}_s\right| \leqslant \frac{\left|\bar{V}_s - R_s \bar{I}_s\right|}{\omega_s}. \tag{32}$$

The inequality (32) represents a constraint on the stator flux magnitude, which is a consequence of the stator voltage limit, and depends on the stator flux angular frequency and the stator current.

In the high speed range the DTC algorithm keeps the torque within the hysteresis band generally applying direct configurations and zero vectors. As the back emf approaches the stator voltage limit, the flux still remains inside the corresponding hysteresis band, whereas the torque demand may be not satisfied. This happens because the DTC algorithm, in the high speed range, gives priority to flux tracking over torque tracking, owing to its intrinsic characteristics. In this case, several consecutive failures of the DTC algorithm occur in driving the torque within the hysteresis band and the torque decreases.

12.2. Flux weakening algorithm. On the basis of the previous considerations it has been found that a suitable acoustic microscope analysis of the output of the torque hysteresis comparator can provide useful information to evaluate if the drive is approaching the base speed.

In a practical implementation of the flux-weakening algorithm the motor behaviour is analysed for N consecutive cycle periods. If no zero vector is applied during that time, then the control algorithm assumes that the flux level is too high for the actual operating conditions. Then, a small decrease of the flux reference is performed. On the contrary, if the DTC algorithm applies at least one zero voltage vector during the N cycle periods, it means that the torque demand is satisfied. As a consequence the control algorithm makes a trial to increase the flux reference. Of course, the flux cannot become lower than a prefixed minimum value or greater than the rated value.

This type of algorithm is useful for traction drives where the input command $T_{command}$ is represented by the gas pedal position. This last in the low speed range corresponds to a constant torque command, whereas in the flux weakening region represents a torque command variable with the speed, so that the output power is constant. For this purpose, the torque reference of the DTC scheme must be adjusted according to the following relationship

$$T^* = T_{command} \frac{\varphi_s^*}{\varphi_{s,rated}}. \tag{33}$$

In the very high speed region, this method could determine a torque demand higher than the maximum torque (29) corresponding to the actual flux φ_s^*. As the maximum torque is proportional to the square of the flux, the torque reference should be set not greater than the following value

$$T_{\max}^* = k_T \left(\varphi_s^*\right)^2. \tag{34}$$

The parameter k_T is nearly constant in the whole flux weakening region and can be determined as the ratio between the maximum torque at the rated flux and the square of the rated flux itself.

12.3. Experimental results. In order to achieve good performance, it has been verified that the DTC sampling frequency should be at least 20 times greater than the update frequency of the flux reference.

Figure 32 shows the behaviour of a motor during a start-up. The final speed is about 400% of the base speed. Initially, the torque command is zero, the motor is at standstill and the flux reference corresponds to the rated value.

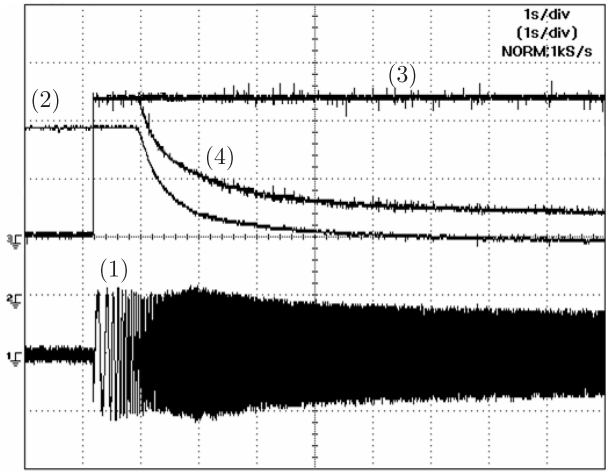

Fig. 32. Starting transient from 0% up to 400% of the base speed. (1) Motor current (20 A/div). (2) Flux reference (0.30 Wb/div). (3) Torque command (10 Nm/div). 4) Torque reference (10 Nm/div)

After the application of a step torque command of rated value, the motor starts up. Until the speed is lower than the base speed, the torque reference equals the torque command. As soon as the base speed is reached, the motor can no more generate the requested torque, and the flux weakening algorithm automatically reduces the flux reference and proportionally the torque reference.

In the constant power speed range, the current is almost constant, according to the operation principle of the flux weakening algorithm. Above the constant power speed range, the torque reference does not follow the behaviour of the flux reference, but decreases proportionally to its square value, according to (34). As can be seen, from a certain speed, the torque reference assumes constant value corresponding to the maximum torque reference, and then the current amplitude decreases.

The experimental results confirm the validity of the proposed flux weakening algorithm whose main advantages can be summarized as follows:

– no need of machine parameters knowledge,
– no need of calculation of the stator flux reference as function of the operating conditions,
– no need of calculation of the base speed, which in general depends on the machine parameters, motor current and DC-link voltage.

13. Comparison between DTC, DSC and FOC schemes

Thirty years ago, in 1971 F. Blaschke presented the first paper on FOC for induction motors. Fifteen years later, in 1984-86 M. Depenbrock and I. Takahashi, presented the first papers on a new control technique called Direct Self Control and Direct Torque Control. Both FOC and DTC-DSC are today becoming the industrial standards for induction motors torque control.

This Section is aimed to give a contribution for a fair comparison between the two control techniques, emphasizing advantages and disadvantages [53]. Because DTC is intrinsically sensorless, a Direct FOC (DFOC) scheme will be considered, instead of a general FOC scheme.

13.1. DFOC and DTC comparison lines. For a fair comparison of the two schemes the following criteria have been adopted.

– The same DSP board for implementing DFOC and DTC schemes.
– The same average switching frequency of the inverter.

A comparison carried out with the same cycle period is not fair enough. In fact, the same cycle period does not allow a suitable use of the basic characteristics of DTC scheme that are the easy implementation and the reduced calculation time.

In both DFOC and DTC schemes the flux estimator has been considered ideal, being the effects due to parameter variations at low speed out of the main aim of this comparison. The quantities employed to evaluate the performance of DFOC and DTC, in steady state and transient conditions, are:

– current and torque ripple values in steady-state operating conditions,
– time response to a step variation of the torque command, at different rotor speeds.

A detailed comparison between the two solutions can be carried out by means of numerical simulations, where secondary effects that could mask the switching behaviour are not present. However, the effects of time discretization and delay caused by the sampling of signals must be taken into account.

The parameters used in the simulations are shown in Table 4. The amplitude of the hysteresis bands have been adjusted in order to achieve a mean inverter switching frequency practically equal to that of DFOC scheme. It is worth noting that, due to the particular modulation strategy adopted, the mean switching frequency of the DFOC scheme is defined as 2/3 of the carrier frequency (6.1 kHz). For DTC, the switching frequency can be defined as the number of switch state changes per second divided by six. With these definitions, the switching frequency of DTC and SVM are directly comparable.

Table 4
Simulation parameters

DFOC Scheme	DTC Scheme
Cycle period = 160 μs	Cycle period = 40 μs
Two-phase modulation	Basic switching table
Technique	Resulting switching frequency = 4.1 kHz

Steady-state performance. With reference to the three-phase rms current ripple the results are shown in Table 5.

Table 5
Three-phase rms current ripple

Torque	DFOC			DTC		
	Speed			Speed		
	1440 rpm	720 rpm	144 rpm	1440 rpm	720 rpm	144 rpm
26.5 Nm	0.64 A	0.63 A	0.58 A	1.10 A	1.57 A	1.46 A
13.25 Nm	0.64 A	0.94 A	0.47 A	1.09 A	1.56 A	1.27 A
0 Nm	0.65 A	0.93 A	0.34 A	1.18 A	1.46 A	1.21 A

As it is possible to see, in all the operating conditions the behaviour of DFOC scheme is characterized by lower values of the three-phase rms current ripple with respect to the DTC scheme. Furthermore, it should be noted that in the high-speed range the DTC scheme operates at a switching frequency lower than 4.1 kHz, even if the amplitude of the hysteresis bands is reduced. This is due to the moderate effect produced by the voltage vectors $\overline{V}_2$ and $\overline{V}_3$ when the torque has to be increased at high speed.

Under the assumption of the same mean inverter switching frequency, the amplitude of the torque ripple in DTC is slightly higher than that of DFOC. However, the oscillations in DFOC scheme are more regular and uniform.

With reference to the current waveforms it can be noted that the harmonic spectrum of DFOC (Fig. 33) shows only the harmonic component corresponding to the modulation cycle period, whereas with DTC scheme the spectrum (Fig. 34) shows a series of harmonics with lower values, but distributed all over the frequency range. According to the current spectrum, DFOC generates a high frequency uniform noise, whereas DTC produces an irregular noise level, which is particularly maddening at low speed.

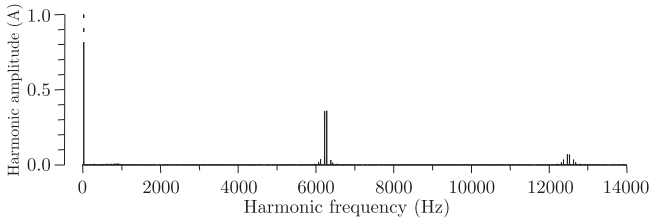

Fig. 33. Stator current harmonic spectrum (DFOC), rated speed, rated torque

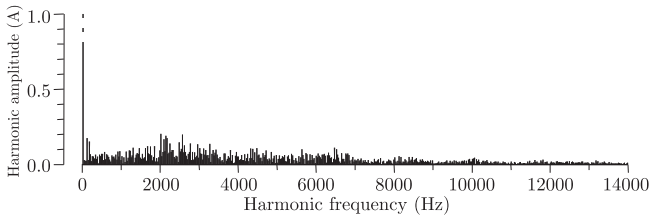

Fig. 34. Stator current harmonic spectrum (DTC), rated speed, rated torque

Transient performance. Figures 35 and 36 show the results obtained for a step variation of the torque command, at 100 rpm. Thee results show that using the DTC scheme a better torque response can be achieved in terms of settling time and maximum overshoot. The different dynamic behaviour is due to the presence of PI regulators in DFOC scheme, which delay the torque response.

From the results obtained it can be concluded that the whole performance of the two schemes is comparable.

DTC might be preferred for high dynamic applications, but it shows higher current and torque ripple. This last drawback could be partially compensated by adopting a DTC-DSVM scheme that requires only a small increase of the computation. Furthermore, the DTC scheme is simpler to be implemented, requiring a very small computational time. Even in low cost DSP platforms, with respect to FOC, it leaves more resources for other tasks (reference generation, communication, management of the user interface, etc.), that nowadays are the prominent part of an industrial drive.

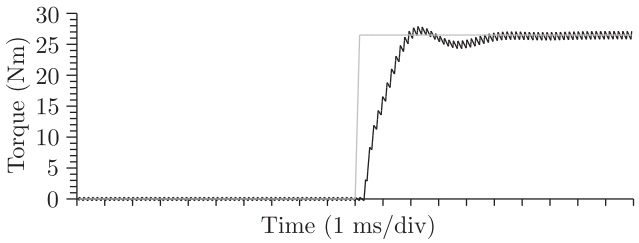

Fig. 35. DFOC torque step response

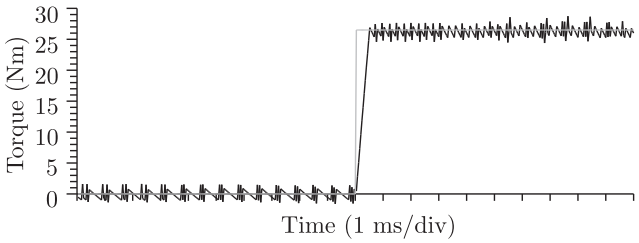

Fig. 36. DTC torque step response

14. Conclusions

The concept of the DTC-DSC technique for IM has been analyzed by means of physical considerations, analytical developments, simulations and experimental results, demonstrating how the stator flux amplitude and the motor torque can be kept under control through the application of the voltage space vectors generated by a VSI.

As in any sensorless IM drive, the performance of a DTC drive deteriorates al low speed. However, it has been illustrated that the use of an improved flux estimator gives the drive good performance even in those operating conditions.

Some improvements to basic DTC scheme have been discussed and a viable solution for flux weakening operation has been presented.

A fair comparison between FOC and DTC, performed on the basis of suitable criteria, concluded that the whole performance of the two schemes is comparable. DTC might be preferred for high dynamic applications. Its higher current and

torque ripple may be partially compensated by adopting a DTC-DSVM scheme. Furthermore, DTC is simpler to be implemented, requiring a very small computational time and low cost DSP platforms.

Appendix

Space vector representation. The "space vector" is a compact and powerful tool for describing a three-phase system of variables a_1, a_2 and a_3.

The instantaneous space vector representation is based on the following transformation:

$$\bar{a} = \frac{2}{3}\left[a_1 + a_2\, e^{j\,\frac{2\pi}{3}} + a_3\, e^{j\,\frac{4\pi}{3}}\right]. \tag{A1}$$

The zero component is defined as

$$a_0 = a_1 + a_2 + a_3. \tag{A2}$$

The inverse transformations are

$$a_1 = \frac{a_0}{3} + \Re_e\,[\bar{a}] \tag{A3}$$

$$a_2 = \frac{a_0}{3} + \Re_e\left[\bar{a}e^{-j\,\frac{2\pi}{3}}\right] \tag{A4}$$

$$a_3 = \frac{a_0}{3} + \Re_e\left[\bar{a}e^{-j\,\frac{4\pi}{3}}\right]. \tag{A5}$$

Space vector representation of the in equations. Under the assumption of no hysteresis, eddy currents and saturation of the magnetic circuit, and the additional assumption of sinusoidal distribution of the stator and rotor windings, the equations of an IM, written in terms of space vectors in a stator reference frame are

$$\bar{v}_s = R_s\bar{i}_s + \frac{d\bar{\varphi}_s}{dt} \tag{A6}$$

$$0 = R_r\bar{i}_r^s + \frac{d\bar{\varphi}_r^s}{dt} - j\,\omega\bar{\varphi}_r^s \tag{A7}$$

$$\bar{\varphi}_s = L_s\bar{i}_s + M\,\bar{i}_r^s \tag{A8}$$

$$\bar{\varphi}_r^s = L_r\bar{i}_r^s + M\,\bar{i}_s \tag{A9}$$

$$T = \frac{3}{2}\,p\,\bar{i}_s \cdot j\bar{\varphi}_s \tag{A10}$$

Combining (A10) with (A8) and (A9), the expression of the torque can be rewritten as follows:

$$T = \frac{3}{2}\frac{pM}{\sigma L_s L_r}\,[\bar{\varphi}_s \cdot j\bar{\varphi}_r^s] \tag{A11}$$

where $\cdot$ represents the scalar product and ω is the rotor angular speed expressed in electrical radians.

Voltage source inverter. A three-phase voltage source inverter can be schematized as in Fig. A1, where V_c is the dc link voltage. The number of the available inverter configurations is $2^3 = 8$.

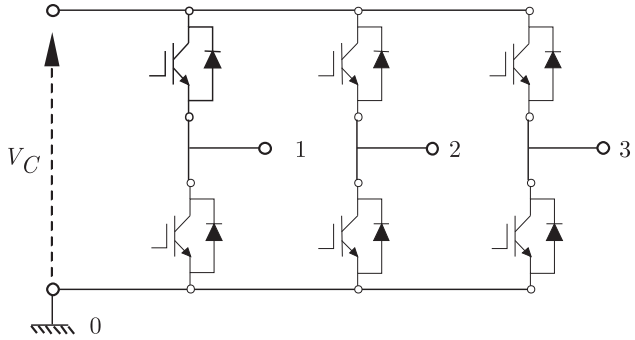

Fig. A1. Schematic representation of a three-phase voltage source inverter

The line-to-neutral voltage vectors corresponding to the 8 inverter states are shown in Fig. A2.

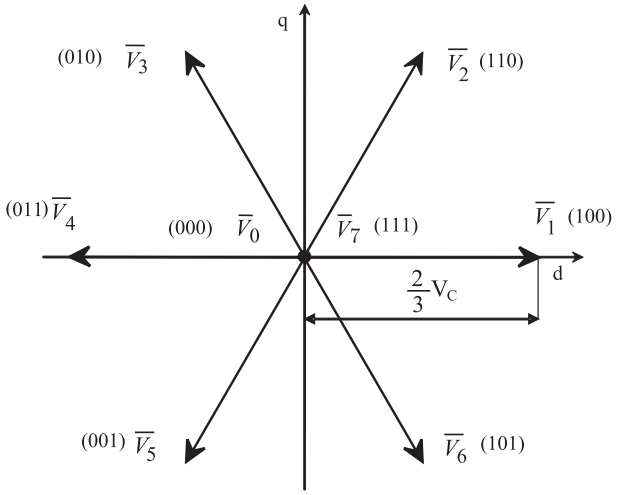

Fig. A2. Inverter voltage space vectors

References

[1] T. Noguchi and I. Takahashi, "Quick torque response control of an induction motor based on a new concept", *IEEJ Tech. Meeting Rotating Mach.* RM84-76, 61–70 (1984), (in Japanese).

[2] I. Takahashi and T. Noguchi, "A new quick-response and high efficiency control strategy of an induction machine", *IEEE Trans. Ind. Applicat.* 22, 820–827 (1986).

[3] I. Takahashi and Y. Ohmori, "High-performance direct torque control of an induction motor", *IEEE Trans. Ind. Applicat.* 25, 257–264 (1989).

[4] M. Depenbrock, "Direkte selbstregelung (DSR) für hochdynamische drehfeldantriebe mit stromrichterspeisung", *ETZ Archive* 7, 211–218 (1985), (in German).

[5] M. Depenbrok, "Direct self-control (DSC) of inverter-fed induction machine", *IEEE Trans. Power Electron.* 3, 420–429 (1988).

[6] M. Depenbrock and A. Steimel, "High power traction drives and convertors", *Proc. Elect. Drives Symp.'90*, 1–9 (1990).

[7] I. Boldea and S.A. Nasar, "Torque vector control (TVC)-A class of fast and robust torque speed and position digital controller for electric drives", *Proc. EMPS'88 Conf.* 15, 135–148 (1988).

[8] T. Ohtani, N. Takada, and K. Tanaka, "Vector control of induction motor without shaft encoder", *IEEE Trans. IA* 28 (1), 157–164 (1992).

[9] D. Casadei, G. Grandi, and G. Serra, "Study and implementation of a simplified and efficient digital vector controller for induction motors", *Conf. Rec. EMD'93*, 196–201 (1993).

[10] D. Casadei, G. Grandi, G. Serra, and A. Tani, "Effects of flux and torque hysteresis band amplitude in direct torque control of induction machines", *Conf. Rec. IECON'94*, 299–304 (1994).

[11] S. Kaboli, E. Vahdati-Khajeh, and M.R. Zolghadri, "Probabilistic voltage harmonic analysis of direct torque controlled induction motor drives", *IEEE Transactions on Power Electronics* 1 (4), 1041–1052 (2006).

[12] D. Casadei, G. Grandi, G. Serra, and A. Tani, "Switching strategies in direct torque control of induction machines", *Conf. Rec. ICEM'94*, 204–209 (1994).

[13] P. Tiitinen, P. Pohkalainen, and J. Lalu, "The next generation motor control method: direct torque control (DTC)", *EPE J.* 5 (1), 14–18 (1995).

[14] J.N. Nash, "Direct torque control, induction motor vector control without an encoder", *IEEE Trans. Ind. Appl.* 33, 333–341 (1997).

[15] M.P. Kazmierkowski and G. Buja, "Review of direct torque control methods for voltage source inverter-fed induction motors", *IECON '03* 1, 981–991 (2003).

[16] B.K. Bose, *Power Electronics and Variable Frequency Drives*, IEEE Press, New York, 1996.

[17] P. Vas, *Sensorless Vector and Direct Torque Control*, Clarendon Press, 1998.

[18] G. Escobar, A.M. Stankovic, E. Galvan, J.M. Carrasco, and R.A. Ortega, "A family of switching control strategies for the reduction of torque ripple in DTC", *IEEE Trans. on Control Systems Technology* 11 (6), 933–939 (2003).

[19] D. Casadei, G. Serra, and A. Tani, "Constant frequency operation of a DTC induction motor drive for electric vehicle", *Proc. ICEM '96 Conf.* 3, 224–229 (1996).

[20] L. Romeral, A. Arias, E. Aldabas, and M.G. Jayne, "Novel direct torque control (DTC) scheme with fuzzy adaptive torque-ripple reduction", *IEEE Trans. on Industrial Electronics* 50 (3), 487–492 (2003).

[21] L.A. Cabrera, M.E. Elbuluk, and D.S. Zinger, "Learning techniques to train neural networks as a state selector for inverter-fed induction machines using direct torque control", *PESC '94 Record.* 1, 233–242 (1994).

[22] D. Casadei, C. Rossi, G. Serra, and A. Tani, "Inverter state selection by neural network in DTC induction motor driver", *SPEEDAM'2000* C(4), 13–18 (2000).

[23] A. Tripathi, A.M. Khambadkone, and S.K. Panda, "Space-vector based, constant frequency, direct torque control and dead beat stator flux control of AC machines", *IECON '01* 2, 1219–1224 (2001).

[24] K.D. Hurst and T.G. Habetler, "A simple, tacho-less, IM drive with direct torque control down to zero speed", *IECON 97* 2, 563–568 (1997).

[25] S. Mir, M.E. Elbuluk, and D.S. Zinger, "PI and fuzzy estimators for tuning the stator resistance in direct torque control of induction machines", *IEEE Trans. on Power Electronics* 13 (2), 279–287 (1998).

[26] M.P. Kazmierkowski and A.B. Kasprowicz, "Improved direct torque and flux vector control of PWM inverter-fed induction motor drives", *IEEE Trans. on Industrial Electronics* 42 (4), 344–350 (1995).

[27] C. Lascu, I. Boldea, and F. Blaabjerg, "A modified direct torque control for induction motor sensorless drive", *IEEE Trans. on Industry Applications* 36 (1), 122–130 (2000).

[28] P.Z. Grabowski, M.P. Kazmierkowski, B.K. Bose, and F. Blaabjerg, "A simple direct-torque neuro-fuzzy control of PWM-inverter-fed induction motor drive", *IEEE Trans. on Industrial Electronics* 47 (4), 863–870 (2000).

[29] D.Casadei, G.Grandi, and G.Serra, "Rotor flux oriented torque-control of induction machines based on stator flux vector control", *Proc. EPE'93 Conf.* 5, 67–72 (1993).

[30] D. Casadei, F. Profumo, G. Serra, A. Tani, and L. Zarri, "Performance analysis of a speed-sensorless induction motor drive based on a constant-switching-frequency DTC scheme", *IEEE Transactions on Industry Applications* 39 (2), 476–484 (2003).

[31] C.J.Bonanno, L.Zhen, and L.Xu, "A direct field oriented induction machine drive with robust flux estimator for position sensorless control", *Conf. Rec. of IAS'95*, 166–173 (1995).

[32] J. Maes and J.A. Melkebeek, "Speed-sensorless direct torque control of induction motors using an adaptive flux observer", *IEEE Trans. on Industry Applications* 36 (3), 778–785 (2000).

[33] T.G. Habetler, F. Profumo, M. Pastorelli, and L.M. Tolbert, "Direct torque control of induction machines using space vector modulation", *IEEE Transactions on Industry Applications* 28 (5), 1045–1053 (1992).

[34] T.G.Habetler, F.Profumo, and M.Pastorelli, "Direct torque control of induction machines over a wide speed range", *IEEE-IAS'92*, 600–606 (1992).

[35] D. Casadei, G. Serra, and A. Tani, "Stator flux vector control for high performance induction motor drives using space vector modulation", *Electromotion Journal* 2 (2), 79–86 (1995).

[36] D. Casadei, G. Serra, A. Tani, and L. Zarri, "Theoretical and experimental analysis of an induction motor drive based on stator flux vector control", *Electromotion Journal* 6 (1–2), 43–48 (1999).

[37] D. Casadei, G. Serra, and A. Tani, "Sensitivity investigation of a speed sensorless induction motor drive based on stator flux vector control", *Conf. Rec. PESC'97*, 1055–1060 (1997).

[38] X. Q. Wu and A. Steimel, "Direct self control of induction machines fed by a double three-level inverter", *IEEE Trans. on Industrial Electronics* 44 (4), 519–527 (1997).

[39] K.B. Lee, J.H. Song, I. Choy, J.Y. Choi, J.H. Yoon, and S.H. Lee, "Torque ripple reduction in DTC of induction motor driven by 3-level inverter with low switching frequency", *PESC 00* 1, 448–453 (2000).

[40] C.A. Martins, X. Roboam, T.A. Meynard, and A.S. Carvalho, "Switching frequency imposition and ripple reduction in DTC drives by using a multilevel converter", *IEEE Trans. on Power Electronics* 17 (2), 286–297 (2002).

[41] Y.S. Lai and J.H. Chen, "A new approach to direct torque control of induction motor drives for constant inverter switching frequency and torque ripple reduction", *IEEE Transactions on Energy Conversion* 16 (3), 220–227 (2001).

[42] D. Casadei, G. Serra, and A. Tani, "Implementation of a direct torque control algorithm for induction motors based on discrete space vector modulation", *IEEE Transactions on Power Electronics* 15 (4), 769–777 (2000).

[43] H.R. Keyhani, M.R. Zolghadri, and A. Homaifar, "An extended and improved discrete space vector modulation direct torque control for induction motors", *PESC 2004* 5, 3414–3420 (2004).

[44] D. Casadei, C. Rossi, G. Serra, and A. Tani, "A predictive voltage-vector selection algorithm in direct torque control of induction motor drive", *Proc. of EPE-PEMC'2002*, on CD (2002).

[45] S.H. Kim, S.K. Sul, and M.H. Park, "Maximum torque control

of an induction machine in the field weakening region", *Conf. Rec. IEEE-IAS'93* 1, 401–407 (1993).

[46] D. Casadei, F. Profumo, G. Serra, A. Tani, and L. Zarri: "Performance analysis of a speed-sensorless induction motor drive based on a constant-switching-frequency DTC scheme", *IEEE Trans. on Ind. Appl.* 39 (2), 476–484 (2003).

[47] F. Khoucha, K. Marouani, K. Aliouane, and A. Kheloui, "Experimental performance analysis of adaptive flux and speed observers for direct torque control of sensorless induction motor drives", *PESC 04* 4, 2678–2683 (2004).

[48] G. Griva, F. Profumo, M. Abrate, A. Tenconi, and D. Berruti, "Wide speed range DTC drive performance with new flux weakening control", *Conf. Rec. PESC'98* 2, 1599–1604 (1998).

[49] H. Grotstollen and J. Wiesing: "Torque capability and control of a saturated induction motor over a wide range of flux weakening", *IEEE Trans. on Ind. Elec.* 42 (4), 374–381 (1995).

[50] A. Tripathi, A.M. Khambadkone, and S.K. Panda, "Dynamic torque control performance of the direct flux control scheme in field weakening range", *IECON '03* 1, 220–225 (2003).

[51] S.H. Kim and S.K. Sul, "Voltage control strategy for maximum torque operation of an induction machine in the field weakening region", *Conf. Rec. IECON'94*, 599–604 (1994).

[52] D. Casadei, G. Serra, A. Tani, and L. Zarri, "A simple method for flux weakening operation of DTC based induction motor drives", *ICEM'2004*, 403–408 (2004).

[53] D. Casadei, F. Profumo, G. Serra, and A. Tani, "FOC and DTC: two viable schemes for induction motors torque control", *IEEE Trans. on Power Electronics* 17 (5), 779–787 (2002).